A Study on the Characteristics of an Oscillating Fluidic Atomizer

K. H. Kim†, K. Kiger* and W. Lee**

Key Words: Nozzle, Liquid Atomization, Jet Oscillation, Oscillating Fluidic Atomizer, Shadowgraph Technique.

Abstract

A unique feature of fluidic atomizers is that the nozzle geometry produces a thin capillary jet which is forced to oscillate on a 2-dimensional plane through the use of a passive feedback mechanism. The objective of the current work is to characterize the influence of the stagnation pressure at the nozzle exit, jet oscillation and stretching on the breakup properties of the capillary ligament. To achieve this, shadowgraph technique is used to measure size, shape, velocity and the number density of the droplets as a function of the position within the spray fan. The breakup length, defined as the radial distance from the breakup point, is analyzed as a function of the non-dimensional parameters. Finally, a kinematic model is developed to simulate the breakup of the oscillating jets at low stagnation pressures. Using the existing jet breakup theories, the model is used to predict the size and diameter distribution of the droplets after primary atomization.

1. Introduction

The current work is on a relatively unexplored type of atomizer which to date has been primarily used as a windshield washer nozzle in automotives. Unlike other common atomizers, the fluidic nozzle issues a liquid jet with a sinusoidal trajectory, which breaks up into small-sized droplets due to the combined effects of stretching the sinusoidal streakline and the commonly studied perturbations and oscillations on the liquid surface.

There are two different kinds of atomizers based on the spray pattern observed at the nozzle exit. The simplest one is the one issuing a circular jet of liquid in the ambient gas air. The other is atomizers generating sheets of liquid which have either flat of conical spray patterns. Some authors also use terms like pressure-swirl nozzles, fan spray nozzles, prefilming air blast nozzles, and rotating disk nozzles, all of which are atomizers issuing sheet of liquid. The atomizers are sometimes also classified based on the techniques used to produce a spray. This classification is especially important when choosing a nozzle for industrial applications. The four main classification of liquid nozzles based on the external agent which causes the jet or sheet to breakup are: pressure nozzles, turbulence nozzles, impact nozzles, and air assisted atomizers. For the direct use to the current work, we will restrict our discussion to liquid jet nozzles. In the present context, we use the term fluidic devices for describing jets with feedback that produce a sweeping or an oscillatory motion of the jet fluid. Other types of nozzles are discussed briefly as follows.

The studies presented were limited to temporal instability analysis where disturbances on the liquid surface are assumed to grow just with time. In reality, most fluid oscillations have an amplitude that is constant with time but grows in a spatial direction. Gaster[1,2] showed that, for small rates of amplification, the disturbance frequencies determined from temporal theory were approximately equal to those of the spatial analysis, and so spatial analysis is needed just for high amplification rates. Keller et al.[3] in his spatial analysis presented important distinctions between liquid jets

(2006년 4월 27일 접수 ~2006년 5월 27일 심사완료)
*Dept. of Mech. Eng., Maryland Univ., U. S. A.
**Research Institute, Dae Ji Metal Co., Korea
†Corresponding Author, Member, Dept. of Mech. Eng., Kyung Hee Univ., Korea
E-mail : kimkh@khu.ac.kr

and spray sheets. Recently, Rangel and Hess[4] investigated non-linear instability of a fluid sheet using a vortex-dynamics model, and Creighton and Lin[5] analyzed spatial spray formation of liquid sheets based on an energy budget. However, for liquid sheets, spatial instability analysis still receives less attention than temporal analysis.

The phenomenon of jet disintegration has been subjected to theoretical and experimental investigation for more than 100 years. Authors have studied the effect of different parameters such as viscosity, surface tension, jet velocity, and nozzle geometry (hydraulic diameter of the nozzle) on the atomization characteristics of the liquid jets injected into a gaseous atmosphere. It applies to combination of liquid (the dispersed phases) and gas (the continuous phase), but for convenience the surrounding gas is usually referred to as air. The properties of jets of most interest are the continuous length, a measure of the growth rate (of the disturbance) and the drop size, which is a measure of the wave number of the most unstable disturbance. Also of interest is the manner in which the jet is disrupted. The work on the 'disintegration of the liquid jet' (also called primary atomization) can be classified into three major categories: linear instability analysis of a laminar jet, non-linear instability analysis of a laminar jet, and turbulent jets.

2. Experimental facilities and measurement techniques

There are several experimental techniques used to study the sprays. The most common ones are PDA (Phase Doppler Anemometry), PIV (Particle Image Velocimetry), Shadow graphic techniques (also called laser light sheet visualization), laser diffraction, and conventional and holographic imaging with automatic image analysis. In the last few years additional diagnostic techniques were developed to study spray characteristics such as: fluorescence dyes for the tagging of particles, simultaneous measurement of drop temperature with drop size and velocity, and particle trajectories in the Lagrangian frame of reference. In the current work, PDA, PIV and shadowgraph techniques are used to characterize the atomizer.

2.1 Test nozzle

The current atomizer is a fluidic device which generates a planar oscillating flow without any moving parts. Fluidic devices[6,7] refer to engineering systems in which fluid motion or displacement transmits significant information as well as power, without any moving mechanical parts. Some examples of common fluidic devices are fluid jet amplifiers and logic elements, vortex valves and sensors, fluid diodes, and capillarity relays.

Fig. 1 shows an enlarged photograph of the current atomizer, and a representation of how the liquid-jet exiting the orifice oscillates in the 2-D plane. From the enlarged photograph of the test section (Fig. 1), whose actual size is not more than 2 mm × 5 mm, it can be seen that the test section is composed of a reservoir on the top, a bistable diffuser section, a pair of feedback paths, and finally a bell-shaped nozzle exit. The fluid enters the test-section through the reservoir, then flows into the bistable diffuser section. The fluid-jet attaches itself to one side of the diffuser and a portion of the jet impinges on the side of the exit to send a pressure wave through the feedback channels. This causes the fluidic-jet to flip over and attach to the other wall. In this manner, a self-repeating limit cycle is formed,

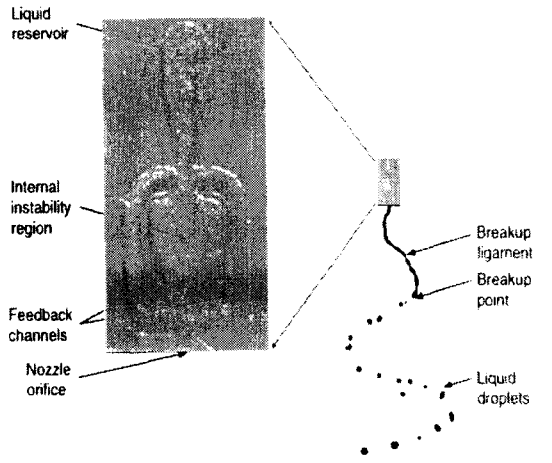

Fig. 1 Magnified image of the nozzle and the corresponding jet ligament

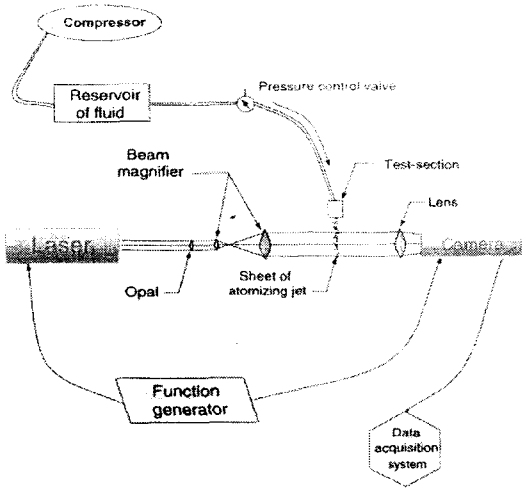

Fig. 2 Experimental set-up for the shadowgraph imaging technique

which results in the observed external oscillatory jet. By controlling the geometry of the nozzle, the rate of oscillation of the ligament can be controlled. The current work is done on a single atomizer provided by Bowles Fluidics Corporation.

2.2 The setup for the shadowgraph measurements

Fig. 2 shows the experimental set-up used for making size and shape measurements and in few cases velocity measurements of the droplets using shadowgraph techniques. The supply consists of a pressure regulated reservoir (3 liters in volume), which uses a steel tank to store the experimental fluid at a fixed pressure. A 500 watt compressor is used to pressurize the steel tank over atmospheric pressures. The pressure is controlled by a precision back pressure regulator with a sensitivity of 1/8" (0.3125 cm) of water. The nozzle consists of a network of fluid channels machined in a thin acrylic plate measuring 2 mm × 5 mm × 0.2 mm. The nozzle is held approximately 1.5 meters above the ground at the same level as the reservoir where the pressure is monitored. The arrangement gives mobility to the test section in two different directions (streamwise and spanwise). A graduated cylinder with an accuracy of 1 ml and a stopwatch with an accuracy of 0.01 sec were used to calibrate the flowrate through the nozzle.

The optical set-up is comprised of a laser, an opal filter, a set of lenses and mirrors to produce a collimated beam of light, and an imaging lens to converge the light onto a CCD (Charged Coupled Device) camera. A pulsed Nd YAG (Clark MXR) laser is used as the illumination source to generate a parallel beam of light. The high speed pulsed laser is capable of up to a 50 kHz repetition rate, although power constraints limit this to 2.5 kHz if uniform intensity pulses are desired. The laser produces sufficiently small (approximately 0.6 μs) pulses of green light (532 nm wavelength) with an energy of 12 mJ per pulse. The small pulse duration helps in freezing the motion of the droplets without blur. An opal filter is used to reduce speckle noise and diffraction rings from the parallel beam coming out of the laser, and this provides a uniform intensity light. The light is then directed through two achromatic lenses that expand and collimate the beam. Theses two lenses are separated by a distance equal to the sum of their focal lengths in order to obtain a parallel output beam. The collimated beam of light, around 4 cm in diameter, passes through the sheet of the atomizing jet onto a lens (Infinity K2 microscope lens) in front of the CCD camera (Kodak Megaplus ES1.0) which collects only the unscattered light. The camera has an image plane of 1008 horizontal pixels by 1018 vertical pixels and is shuttered to capture 15 image pairs per second. The image area was approximately 20 mm x 16 mm. A function generator is used to synchronize the timing of the laser pulse and the exposure of the camera. A time separation of 400 μs was set between the image pairs.

The experimental setup and procedure discussed in section 2.2 is used to take the shadowgraph images of the atomizing fluidic-jet at different locations and flowrates to extract information on location, size, shape, velocity and number density of the droplets.

2.3 Data processing technique

The images also give information about the breakup length and spread-angle of the spray. This section presents a brief discussion of the processing procedures associated with the shadowgraph method. First, the raw images of the jet are obtained (as shown in Fig. 3a), and a consistent threshold level is set to remove background

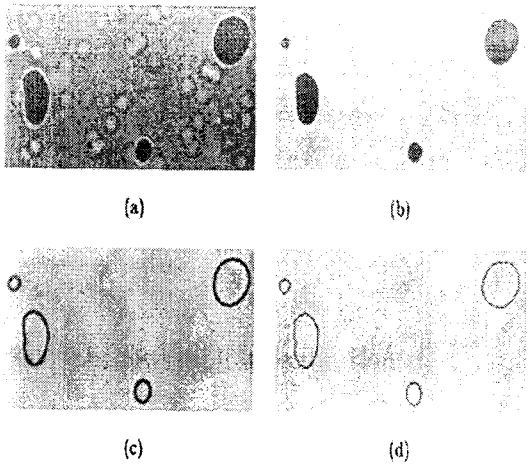

Fig. 3 Image processing procedure. (a) The original image, (b) Threshold scaling to eliminates background noise, (c) edge detection, and (d) thinning, which converts the isolated droplets into single-pixel-thick "skeleton" form

noise caused by imperfections in the beam and lens system. This procedure results in high-contrast images of the deforming ligaments and droplets (Fig. 3b). Different image processing techniques are then used to convert the image into a form in which the droplet's size and shape can be numerically quantified. A sobel filter is used to identify the high-contrast edges of the droplets (Fig. 3c). A thinning procedure (Fig. 3d) is used to convert the gradient regions generated by the sobel filter into single-pixel-thick "skeleton" form. All continuous, closed loop forms are then identified as perimeters of droplets or ligaments, and their area, perimeter, and centroid are recorded for statistical analysis. For velocity calculations, the location of a single droplet is determined in two successive images acquired Δt = 400 μs apart. The velocity is then calculated as the centroid displacement divided by the time. Due to the requirement of identifying droplet pairs between successive images, using the shadowgraph technique, velocity measurements could only be obtained under conditions where relatively few (~100) particles were present (or at relatively low speeds ~0.5 m/s).

2.4 Shadowgraph image calibration

A calibration of the sizing method was performed using a standard PattersonGlobe reticle, which consisted of a glass substrate etched with 10 precision disks of known size (see Fig. 4a). The disk images were digitized and processed in the same manner as the spray images, and the results compared to the known size are shown in figure 4b. As can be observed, there is a slight tendency for the droplets to be underestimated, but the error is everywhere less than 6%, with an average around 1.9%. Table 1 presents the actual versus experimentally measured values for the diameter of the seven reticles, and the corresponding error in measurement. A negative error shows that the measurement technique underestimates the respective diameter of the reticle. To understand how far does the smallest droplet (100 μm) needs to be from the focal plane for it to disappear, a plot of the

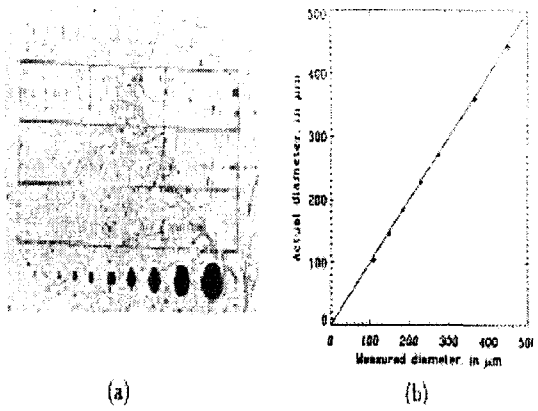

Fig. 4 Shadowgraph calibration (a) Image of Patterson Globe reticle, (b) experimentally measured vs. actual disk sizes

Table 1 Actual versus experimentally measured values for the diameter of the calibration reticles

Actual diameter, μm	Measured diameter, μm	% error
110	103.5	-5.9
150	146.3	-2.5
184	184.2	+0.1
230	227.9	-0.9
275	271.4	-1.3
365	360.2	-1.3
450	442.5	-1.7

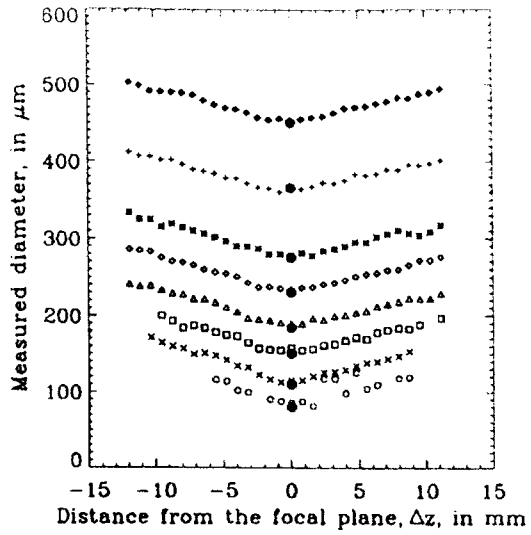

(a)

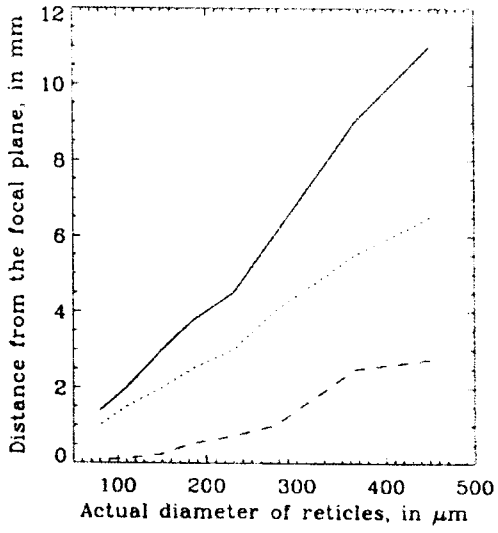

(b)

Fig. 5 (a) Measured diameter of the Patterson Globe reticles at varying distance from the focal plane (b) Distance from the focal plane versus actual diameter of the reticles at three levels of accuracy

measured diameter vs. the distance from the focal plane is presented in Fig. 5a. The diameter calculation is overestimated as one moves away from the focal plane. The diameter for a 300 μm disk (around the mean value of the droplet values for the current experiments) has an accuracy within 2% when moved about 1 mm from the focal plane, within a 5% accuracy as far as 4 mm from the focal plane, and has within a 10% accuracy for as far as 7 mm. For the smallest disk of 110 μm, the diameter calculation is 10% accurate as far as 1.5 mm. Fig. 5b presents the distance from the focal plane vs. the measured diameter plot for an accuracy of 2%, 5%, and 10%. So the depth of focus is not much of an issue for the current experimental measurements.

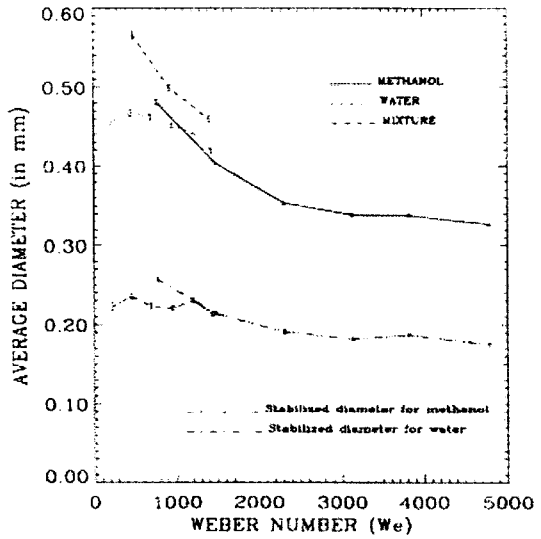

(a) $\overline{D}$ vs Reynolds Number

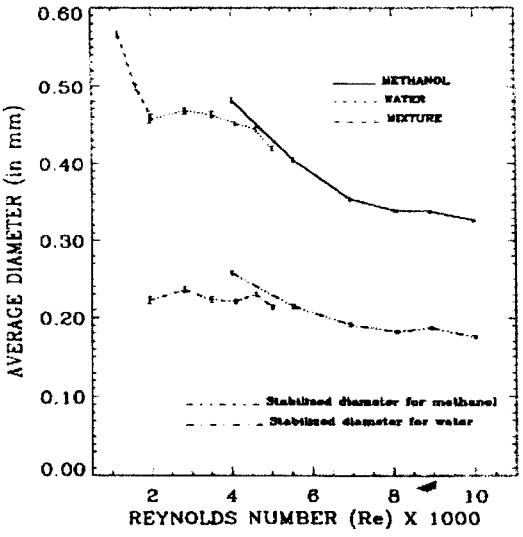

(b) $\overline{D}$ vs Weber Number

Fig. 6 Change in average diameter of the first generation droplets with non-dimensional parameters: *Re* and *We*

3. Results and discussion

Using shadowgraph techniques, the mean diameters (number mean, D_{10}, area mean, D_{20}, volume mean, and the sauter mean, D_{32}) were calculated for the three fluids for different downstream positions over the flowrate range of 10~45 cc/min. Fig. 6 shows the variation of number mean diameters of the first generation droplets with the non-diameter parameters: Reynolds number(*Re*), and Weber number(*We*). Fig. 6 also compares the diameter of the first generation droplets with the diameter of the droplet when the breakup has stabilized. The Reynolds and Weber numbers here are based on the hydraulic diameter and the velocity at the nozzle exit. To get a value for the mean diameter of the first generation droplets, an average of the diameter of all the droplets within a bin size of 4.8 mm (along x direction) by 2.4 mm (in y direction) were taken, where the bin was suitably placed such that the lower x-coordinate of the bin is as close to the breakup point as possible (generally the center of the bin was at x = 6.4 mm, y= 0 mm). From Fig. 6a it can be seen that the droplet size decreases with an increase in Reynolds number, which represents an increase in inertia of the droplets and hence presents additional energy to fracture the droplets into small sizes. The Weber number, which is a ratio of inertia and surface tension forces, also affects the droplet size. Fig. 6b shows that in general, there is a decrease in size with increasing Weber number, signifying increased atomization due to a decrease in surface tension. The steep slope for *We* < 1500 corresponds to a rapid increase in the smaller satellite droplets formed during the transition to a turbulent ligament breakup process. It can also be observed from these figures that no conclusive scaling law can be produced to uniformly collapse the data acquired, even for the small number of samples represented by the current measurements. It is therefore likely that any model would have to incorporate both of these non-dimensional parameters to accurately reproduce the atomizer behavior. Fig. 7 shows the first generation droplets and the droplets after breakup stabilization on a *We* vs. *Re* plot. The droplets have been classified into different size class to better understand the correlation

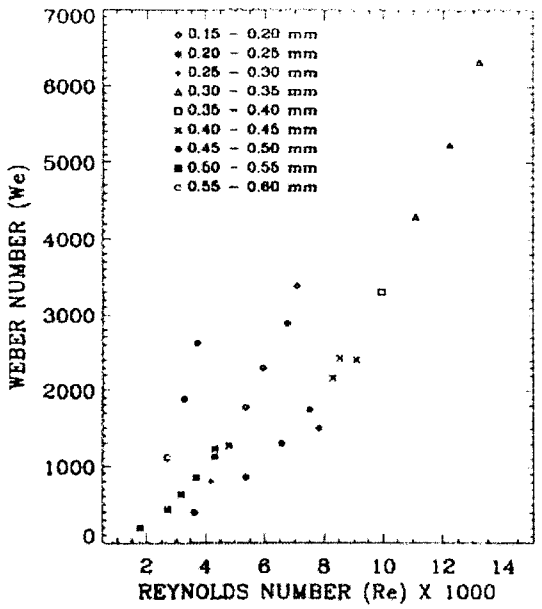

Fig. 7 The classification of the first generation and the "breakup-stabilized" droplets in different size range, on a *We* vs. *Re* plot

between the diameter of the droplets and the non-dimensional numbers (the Reynolds and Weber numbers). A rough grouping of the droplets of the same size class can be clearly seen on the Weber number vs. Reynolds number plot in Fig. 7.

Fig. 8 and 9 show the cross-stream number diameter profiles of water and methanol for six different pressures and at four different downstream positions for every pressure. from the plots, it can be seen that the average diameter tends to decrease with increasing pressure (also confirmed by Fig. 6) across most of the span. The second feature to note is that with the exception of the outer edges of the spray fan, the size decreases as one moves downstream for a given pressure due to the breakup of the ligaments and large droplets that occurs in the early region of the flow. For all of the water cases, the diameter continues to change with downstream position, indicating that the breakup process is not yet complete. For the methanol case, which extends much further into the turbulent regime than the water case, the diameter appears to reach a constant value for the 172.3 and 206.8 kPa examples. The profiles for the laminar and the transitional states

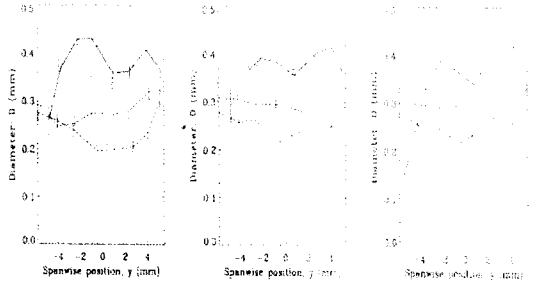

(a) 34.4 kPa (b) 68.9 kPa (c) 103.4 kPa

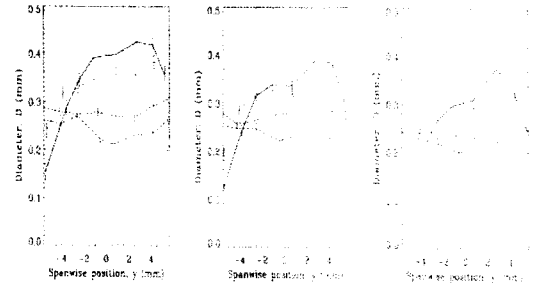

(d) 137.8 kPa (e) 172.3 kPa (f) 206.8 kPa

Fig. 8 Number mean diameter(D_{10}) across the span of the jet, for water, for six different pressures covering a flowrate range of 10~45 cc/min

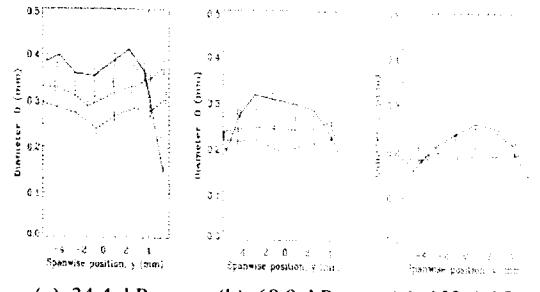

(a) 34.4 kPa (b) 68.9 kPa (c) 103.4 kPa

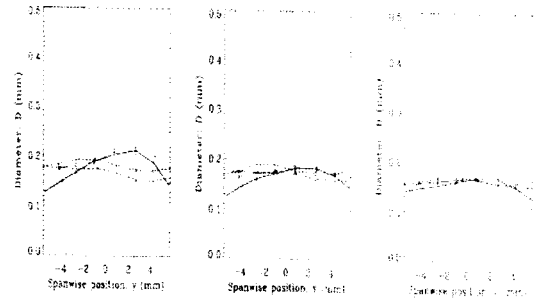

(d) 137.8 kPa (e) 172.3 kPa (f) 206.8 kPa

Fig. 9 Number mean diameter(D_{10}) across the span of the jet, for methanol, for six different pressures covering a flowrate range of 10~45 cc/min

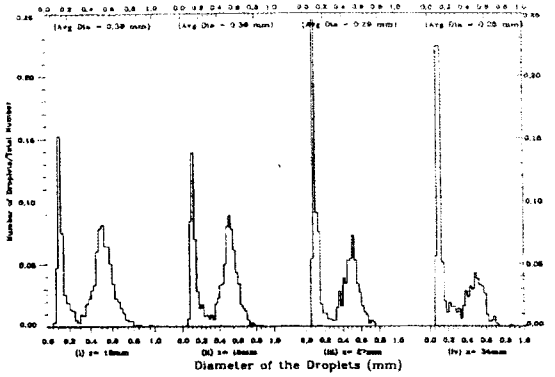

(a) 34.4 kPa

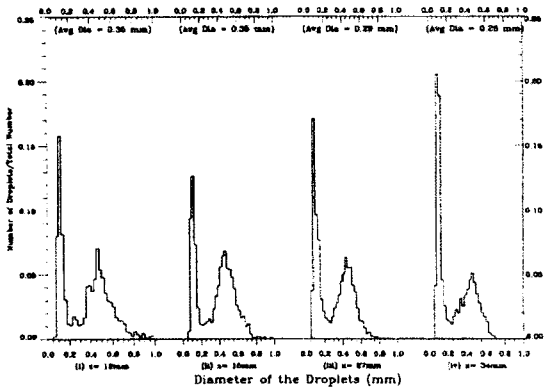

(b) 68.9 kPa

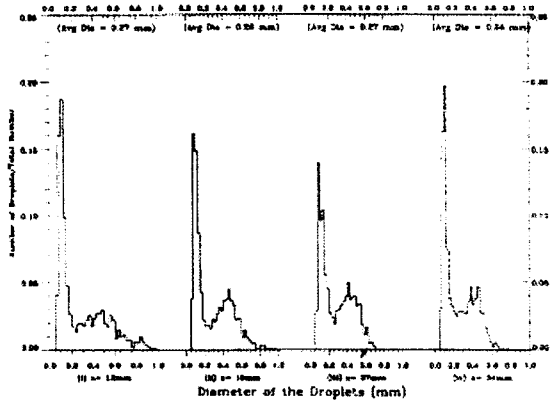

(C) 103.4 kPa

Fig. 10 Diameter distribution histograms for water, for three different pressures and at four different downstream positions

always start with a slight dip in the mean size at the center of the plot, an increase on either side (usually with some asymmetry), and then a decrease on the edges. As one moves downstream from these initial

conditions, the diameter on the centerline continues to drop, while the peaks of the profiles erode only slightly and move further outward, leaving a nearly uniform profile that dips slightly near the center. For the turbulent regime exemplified by the higher pressure methanol cases (Fig. 9c, d, e, f), there is no dip observed in the initial size near the centerline, but instead the profiles across the span show a concave-down type behavior. The final profiles for these cases exhibit a relatively flat shape across the entire width of the span. The area mean and volume mean diameter plots are very similar to the number mean diameter plots showing relatively little variance in the drop size.

In order to understand some of these observed features with increases in flowrate, the corresponding diameter distribution histograms are show in Fig. 10, for water and methanol at three of the selected pressures. These readings were taken for a bin size of 4 mm (along x direction) by 8 mm (in y direction), with the center of the bin at y-0 and an x value corresponding to of satellite droplets more than the total volume of the main droplets. The peak for the main droplets is around, D = 1.9d, close to the value of D = 1.89d proposed by Rayleigh's classical results. The first moment of the number distribution of the diameter gives a value of

$$D = 1.17d$$

lower than that found by earlier analysis. So the earlier analysis is closer to the experimental values.

4. Conclusions

The oscillating fluidic atomizer was studied using two different experimental techniques. The size of the droplets decreased while the average velocity increased with an increase in the supply pressure. Three breakup regimes were identified as laminar, with Rayleigh 'varicose' type of breakup, turbulent, characterized by the presence of large number of small satellite droplets forming near the nozzle, a small breakup length, and transitional with properties in-between the laminar and turbulent cases. D_{10} varies from around 0.15 mm to 0.4 mm depending on Re and We. For the small range of exit velocity studied, the breakup length increases with Reynolds number and Weber number which is consistent with the observations of other authors in that range of Reynolds and Weber numbers. The low pressure kinematic model quite closely predicted the drop size.

5. References

(1) Gaster, M., "A note on the relation between temporally-increasing and spatially-increasing disturbances in hydrodynamic stability", J. Fluid Mechanics, 14, 1962, pp. 222~224.

(2) Gaster, M., "Growth of disturbances in both space and time", Phys. Fluids, 11, 723., 1968.

(3) Keller, J.B., Rubinow, S. F., and Tu, Y. O., "Spatial instability of a jet", Phys. Fluids, 16, 1973, pp. 2052~2055.

(4) Rangel, R. and Hess, C., "Nonlinear spatial instability of fluid sheet", Technical report, AIAA Paper No.90-0118., 1990.

(5) Creighton, B. and Lin, S. P., "Mechanism of atomization of liquid sheets", Atomization and Sprays, 1(2), 1991, pp. 187~197.

(6) Brown, F. T., "Advances in fluidics", The American Society of mechanical Engineers, New York., 1967.

(7) Conway, A., "A guide to fluidics", Macdonald and Co. (Publishers) Ltd., London., 1971.